Checkerboard-Mask Coronagraphs for High-Contrast Imaging

Robert J. Vanderbei

Operations Research and Financial Engineering, Princeton University

rvdb@princeton.edu

N. Jeremy Kasdin

Mechanical and Aerospace Engineering, Princeton University

jkasdin@princeton.edu

David N. Spergel

Astrophysics, Princeton University

dns@princeton.edu

ABSTRACT

We present yet another new family of masks for high-contrast imaging as required for the to-be-built terrestrial planet finder space telescope. We call these masks *checkerboard* masks. They consist of two *barcode* masks, one rotated 90° with respect to the other. Each barcode mask provides contrast to the 10^{-5} level. The checkboard mask then achieves a 10^{-10} level of contrast everywhere except along the two axes of symmetry where the contrast remains at the 10^{-5} level. With these designs, we are able to reduce the inner working angle to $2\lambda/D$ for each barcode which translates to $2\sqrt{2}\lambda/D$ along the diagonal of the associated checkerboard mask. We show that by combining a Lyot-plane checkboard mask with an image-plane occulter we can achieve even tighter inner working angles, although as with occulting designs in general pointing error and stellar size become nontrivial issues. Checkerboard masks can be thought of as the binary-mask analogue of Nisenson's apodized square aperture concept.

Subject headings: planetary systems — instrumentation: miscellaneous

1. Introduction

Following our previous work on pupil-plane masks for high-contrast imaging in the context of terrestrial planet finding (see Kasdin et al. (2003); Vanderbei et al. (2003b,c)), we present in this paper further new pupil masks as well as some pupil-plane/image-plane combinations of masks. Most of our earlier pupil-plane mask designs have an inner working angle (*IWA*) of $4\lambda/D$, which implies a main mirror in the 12 m range (as usual, λ is wavelength and D is aperture). One of the main objectives leading to the designs presented in this paper was to decrease significantly this inner working angle. If the inner working angle can be reduced to $2\lambda/D$, then the main mirror can be dropped down to the 6 m range and still be capable of studying the same set of stars. This is our goal.

One of the pupil masks presented here achieves a contrast ratio of 10^{-10} in four rectangular regions of the image plane given by $\{(\xi,\zeta) : 2 < |\xi| < 20,\ 2 < |\zeta| < 20\}$. The points of high-contrast that are closest to the center of the star's image occur along the diagonals and therefore correspond to an inner working angle of $2\sqrt{2} = 2.8\lambda/D$.

The masks considered in this paper consist of rectangular arrays of rectangular openings. We call them *checkerboard* masks. They can be built as two identical striped masks one placed on top of the other but oriented so that the stripes on one mask are orthogonal to the stripes on the other (see Figure 1). We call the striped masks *barcode* masks (see Kasdin et al. (2004)). Each barcode mask need only provide a contrast ratio of 10^{-5}—it is then guaranteed that the two-mask overlay can achieve a contrast of 10^{-10}. This is important since it is quite feasible to check in a laboratory that a barcode mask achieves 10^{-5} but is difficult, if not impossible, to check that a mask achieves 10^{-10} on the ground. Note that this performance guarantee assumes that the Fraunhofer approximation is adequate and that the instrument has a wavefront amplitude and phase control system that is able to achieve the required extreme contrast. These are very serious issues that we and others are working on and will report on in other papers.

We show that one can get an even tighter IWA of $1.4\sqrt{2} = 2.0\lambda/D$ by placing a rectangular pupil-plane mask in the Lyot plane of a traditional coronagraph and using an image-plane hard occulting mask consisting of a "plus-sign" shape, $\{(\xi,\zeta) :\ |\xi| < 0.6,\ |\zeta| < 0.6\}$. We show that such a coronagraph can tolerate pointing errors as large as about $0.05\lambda/D$.

Finally, in the interest of producing an on-axis coronagraph, we present a Lyot-plane rectangular pupil mask which includes a 2% 4-vane spider. A similar spider can then be placed in the entrance pupil and provide the opportunity to place a small secondary mirror at the center of the plane. Having such a spider over the entrance pupil provides the possibility of building an all-mirror on-axis system and in this way greatly reducing the negative effects of differential polarization that are a concern with off-axis designs. Of course, a 2% secondary mirror is very small

and perhaps not practical.

2. Pupil Apodizations and Masks

In this paper, we assume that telescope optics follow the Fraunhofer approximation. Hence, given a pupil plane apodization function $0 \leq A(x,y) \leq 1$, the image-plane electric field corresponding to an on-axis point source is given by the two-dimensional Fourier transform of the apodization function:

$$E(\xi,\zeta) = \widehat{A}(\xi,\zeta) := \iint e^{2\pi i(\xi x+\zeta y)} A(x,y) dy dx. \tag{1}$$

If the apodization function takes only the values zero and one, then the function represents a *mask*. The intensity in the image plane is the square of the magnitude of the electric field. For an on-axis point source, this intensity function is called the *point spread function (psf)*.

Certain performance metrics guide our choice of the best pupil apodization (or mask). For example, the inner working angle ρ_{iwa} and outer working angle ρ_{owa} specify the desired high-contrast region. For circularly symmetric designs, high contrast is specified by the requirement that

$$|E(\xi,\zeta)|^2/|E(0,0)|^2 \leq 10^{-10}, \qquad \rho_{\text{iwa}} \leq \sqrt{\xi^2+\zeta^2}\rho_{\text{owa}}. \tag{2}$$

Another important consideration is the amount of light that gets into the main lobe of the psf. We express this as a fraction of the total light available to an open unapodized aperture and call it the *Airy throughput* denoted $\mathcal{T}_{\text{Airy}}$. Finally, the full-width half-max (FWHM) of the main lobe of the psf is an important measure of the sharpness of the psf. For comparison purposes, we review these metrics for some simple apodizations.

2.1. Clear Aperture

For an open circular aperture, FWHM $= 1.02$, $\mathcal{T}_{\text{Airy}} = 84.2\%$, and, if we define the inner working angle as the angle of the first null, which defines the border of the Airy disk, then $\rho_{\text{iwa}} = 1.24$. Of course, with this definition of ρ_{iwa}, the contrast constraint (2) is not satisfied. This is bad. If we choose $\rho_{\text{owa}} = \infty$ and then pick the smallest ρ_{iwa} for which the contrast constraint (2) is satisfied, we get $\rho_{\text{iwa}} = 743$, far too large for a practical planet finding system.

2.2. Optimal Circularly Symmetric Apodization

In Vanderbei et al. (2003b), we presented a circularly symmetric apodization that we found by maximizing $E(0,0)$, which is a simple surrogate for Airy throughput, subject to contrast constraints as given by (2) and some mild smoothness constraints on the apodization function. In this way, we found an apodization function for which FWHM $= 2$, $\rho_{\text{iwa}} = 4$, $\rho_{\text{owa}} = \infty$, and $\mathcal{T}_{\text{Airy}} = 9\%$. Except for the imposition of smoothness constraints, this apodization represents the best that one can expect to achieve with any circularly symmetric apodized or shaped pupil design. In particular, the Airy throughput of 9% should be thought of as an upper bound on the throughput one can obtain if one wishes there to be no light brighter than 10^{-10} outside of the inner working angle of $4\lambda/D$. The get higher throughput, one must accept either a larger inner working angle, a smaller outer working angle, or a design in which the dark zone is not an entire annulus. If we assume that a throughput of 9% is adequate, then the only downside to this design is that it is not possible with current technology to apodize a pupil to the level of precision required.

2.3. Concentric Ring and Spiderweb Masks

Also in Vanderbei et al. (2003b) we show that, if one relaxes the smoothness constraint, then the optimal solution turns out to be zero/one-valued, i.e., a mask. The metrics for this design are: FWHM $= 1.9$, $\rho_{\text{iwa}} = 4$, $\rho_{\text{owa}} = 60$, and $\mathcal{T}_{\text{Airy}} = 9\%$. The only downside to this design is that the mask consists of concentric rings that must be supported somehow. If they are laid on glass, then there is concern that imperfections in the glass will introduce too much scattered light. Another possibility is to use a large number of spiders to support the rings. If the number of spiders is large enough, say more than 150, then a reasonably large dark zone is preserved. But, again, concerns about manufacturability resurface. Also, throughput is reduced somewhat by the presence of the spider vanes.

3. Barcode and Checkerboard Pupil Masks

In the previous section, we reviewed our prior work on circularly symmetric pupil mask design. With those designs, the best we were able to do is to get an inner working angle of 4 and an Airy throughput of 9%. Also, manufacturability was an issue in all of those designs. In this section, we introduce new pupil designs that break the $\rho_{\text{iwa}} = 4$ barrier and are more amenable to manufacture.

We should note that one can also break the 9% throughput barrier by limiting the discovery

zone to less than 360°. The original Spergel pupil (Spergel (2000)) is an example of this as are some of the designs we have developed earlier (see, e.g., Figure 8 in Vanderbei et al. (2003a)).

If the apodization function depends only on one of the coordinates (either x or y), then we say that it is a *one-dimensional apodization* or a *one-dimensional mask*. We also refer to one-dimensional masks as *barcode* masks. This family of masks were studied in Kasdin et al. (2004). In this paper, we are interested in masks that correspond to the tensor product of a pair of one-dimensional masks:

$$A = A_x \otimes A_y \qquad \Leftrightarrow \qquad A(x,y) = A_x(x)A_y(y). \tag{3}$$

The electric field corresponding to a tensor product is itself a tensor product:

$$E = \widehat{A} = \widehat{A_x \otimes A_y} = \widehat{A_x} \otimes \widehat{A_y}. \tag{4}$$

In other words,

$$E(\xi,\zeta) = \widehat{A_x}(\xi)\widehat{A_y}(\zeta). \tag{5}$$

Tensor products of smooth apodizations were first proposed for terrestrial planet finding in Nisenson and Papaliolios (2001).

Since intensity is the square of the magnitude of the electric field, it follows that for a contrast of 10^{-10}, we seek apodization functions that provide the following contrast inequalities:

$$|E(\xi,\zeta)| \le 10^{-5}E(0,0), \qquad (\xi,\zeta) \in \mathcal{O}, \tag{6}$$

where $\mathcal{O}$ denotes the points in the image plane at which high contrast is to be achieved. Suppose as before that the apodization function is a tensor product. If the set $\mathcal{O}$ is a *generalized rectangle*

$$\mathcal{O} = \{(\xi,\zeta) : \ \xi \in \mathcal{O}_\xi, \ \zeta \in \mathcal{O}_\zeta\} \tag{7}$$

(i.e., $\mathcal{O} = \mathcal{O}_\xi \times \mathcal{O}_\zeta$), then the contrast inequalities can be achieved by giving two one-dimensional apodizations that each achieve a contrast ratio of only 10^{-5}:

$$|\widehat{A_x}(\xi)| \ \le \ 10^{-2.5}\widehat{A_x}(0), \qquad \xi \in \mathcal{O}_\xi, \tag{8}$$

$$|\widehat{A_y}(\zeta)| \ \le \ 10^{-2.5}\widehat{A_y}(0), \qquad \zeta \in \mathcal{O}_\zeta. \tag{9}$$

Figure 1 shows a checkerboard mask corresponding to $\mathcal{O}_\xi = \mathcal{O}_\zeta = \{\xi : 2 \le |\xi| \le 25\}$. The mask has a 28.1% open area. Its *Airy throughput*, defined as

$$\mathcal{T}_{\text{Airy}} = \int_{-\xi_0}^{\xi_0}\int_{-\xi_0}^{\xi_0} |E(\xi,\zeta)|^2 d\zeta d\xi, \tag{10}$$

where ξ_0 denotes the inner working angle for the barcode mask, is 15.1%. The sharpness measured along the diagonal is FWHM $= 0.94 * \sqrt{2}$ and its inner working angle is $\rho_{\text{iwa}} = 2\sqrt{2}$. This design breaks both the $4\lambda/D$ inner working angle limit and the 9% Airy throughput limit. These gains come at the expense of introducing a $+$-shaped "diffraction spike" at the 10^{-5} level that extends beyond the inner working angle as well as a smallish outer working angle.

Figure 2 shows another checkerboard mask. For this mask, a 2% central obstruction was imposed on the design. With such a central obstruction (and implied spiders) one can hang and hide a small secondary mirror and therefore build a telescope with an on-axis optical path. In this design, we have used $\mathcal{O}_\xi = \mathcal{O}_\zeta = \{\xi : 2 \leq |\xi| \leq 11\}$. The mask has a 17.2% open area. Its *Airy throughput*, is 5.3% and its inner working angle (measured along the diagonal) is $\rho_{\text{iwa}} = 2\sqrt{2}$. It remains to be determined whether the reduced throughput and the smallness of the central obstruction outweigh the advantages of having an on-axis design.

We end this section by pointing out that PSFs associated with these masks (and in fact all pupil-plane masks) depend on wavelength only in that the inner working angle is measured in units of λ/D, where λ is wavelength and D is aperture. Hence, measured in radians, at longer wavelengths the inner working angle is correspondingly larger.

4. A Lyot Coronagraph

Consider an imaging system consisting of an entrance pupil, a first image plane, a reimaged (Lyot) pupil plane, and a final image plane (containing an imaging device). We assume that each of the first three planes can be apodized/masked. Following Kuchner and Traub (2002), we let A denote the mask function for the entrance pupil, $\hat{M}$ the mask function for the first image plane, and L the mask function for the Lyot pupil.

The electric field at point (ξ, ζ) in the final image plane corresponding to an off-axis point source is a composition of mask multiplication and Fourier transformation:

$$\mathcal{F}\left(L \cdot \mathcal{F}\left(\widehat{M} \cdot \mathcal{F}\left(A \cdot F_{-\xi_0,-\zeta_0}\right)\right)\right)(\xi,\zeta) = \widehat{L} * \left(\widehat{M} \cdot (\widehat{A} * \delta_{\xi_0,\zeta_0})\right)(\xi,\zeta), \tag{11}$$

where $F_{-\xi_0,-\zeta_0}$ denotes the electric field at the entrance pupil corresponding to a point source from direction (ξ_0, ζ_0), δ_{ξ_0,ζ_0} denotes a unit mass delta function at (ξ_0, ζ_0), hats denote Fourier transforms and stars denote convolutions.

It is easy to see that if each of L, M, and A are tensor products ($L = L_x \otimes L_y$, $M = M_x \otimes M_y$, $A = A_x \otimes A_y$), then the electric field again factors into a product of electric fields:

$$\widehat{L} * \left(\widehat{M} \cdot (\widehat{A} * \delta_{\xi_0,\zeta_0})\right)(\xi,\zeta) = \widehat{L_x} * \left(\widehat{M_x} \cdot (\widehat{A_x} * \delta_{\xi_0})\right)(\xi) \quad \widehat{L_y} * \left(\widehat{M_y} \cdot (\widehat{A_y} * \delta_{\zeta_0})\right)(\zeta) \tag{12}$$

We use this factorization to greatly simplify the coronagraph optimization problems described in the next section.

5. Lyot Coronagraph Optimization Problem and Numerical Results

As in our previous papers (Kasdin et al. (2003); Vanderbei et al. (2003b,c)), we use numerical optimization to maximize some measure θ of throughput subject to imposed contrast constraints. For the designs presented in this section, we solve the following one-dimensional barcode optimization problem:

$$\begin{array}{lll} \text{maximize} & \theta & \\ \text{subject to} & \theta \;\le \widehat{L} * \left(\widehat{M} \cdot (\widehat{A} * \delta_{\xi,\zeta})\right)(\xi,\zeta), & (\xi,\zeta) \in \mathcal{O}, \\ & \left|\widehat{L} * \left(\widehat{M} \cdot (\widehat{A} * \delta_0)\right)(\xi,\zeta)\right| \;\le \dfrac{\widehat{L} * \left(\widehat{M} \cdot (\widehat{A} * \delta_{\xi,\zeta})\right)(\xi,\zeta)}{10^{2.5}}, & (\xi,\zeta) \in \mathcal{O}. \end{array} \tag{13}$$

The first set of constraints say that θ is a lower bound on the electric field of a unit off-axis source (i.e, a planet as bright as a star) as the off-axis source varies over the high-contrast region. The second set of constraints say that the magnitude of the electric field at $\xi \in \mathcal{O}$ due to an on-axis star is smaller than the electric field at the same point in the image plane due to a much fainter planet whose image is centered at this point ξ. The functions L, M, and A are functions of a single real variable and represent either the x or the y component of a tensor product that one forms to make the final two dimensional image. By specifying prescribed functions for A and M (actually, $\widehat{M}$) we can optimize only the function L. In this case, the problem is an infinite dimensional linear programming problem. Discretizing the image and pupil planes reduces the problem to a finite dimensional linear programming problem that can be solved numerically.

We now give two specific examples of Lyot coronagraphs. For the first example, we specify

that

$$A(x) = \begin{cases} 1 & |x| \leq \frac{1}{2} \\ 0 & \text{otherwise} \end{cases} \tag{14}$$

$$\widehat{M}(\xi) = \begin{cases} 1 & 0.6 \leq |\xi| \leq 84 \\ 0 & \text{otherwise} \end{cases} \tag{15}$$

$$|L(x)| \quad \begin{cases} \leq 1 & |x| \leq \frac{1}{2} \\ = 0 & \text{otherwise} \end{cases} \tag{16}$$

$$\mathcal{O} = \{\xi : 1.4 \leq |\xi| \leq 21\} \tag{17}$$

The optimal barcode mask is shown in Figure 3 together with the corresponding checkerboard mask. This coronagraph has an off-axis Airy throughput of 6.2% and its inner working angle is $\text{FWHM} = 1.4\sqrt{2}$.

The second example is the same as the first except that we impose a central obstruction in the pupil-plane masks:

$$A(x) = \begin{cases} 1 & 0.01 \leq |x| \leq \frac{1}{2} \\ 0 & \text{otherwise} \end{cases} \tag{18}$$

$$|L(x)| \quad \begin{cases} \leq 1 & 0.01 \leq |x| \leq \frac{1}{2} \\ = 0 & \text{otherwise} \end{cases} \tag{19}$$

The optimal barcode mask is shown in Figure 4 together with the corresponding checkerboard mask. This coronagraph has an off-axis Airy throughput of 3.5% and, again, the inner working angle is $\rho_{\text{iwa}} = 1.4\sqrt{2}$.

Since the designs presented in this section involve an image plane mask, the associated PSFs depend on wavelength in a more complicated way than the designs given in Section 3. To test this wavelength dependency, we did a crude test. We computed the image of our usual 3-planet system using four different wavelengths, two shorter (85% and 90%) and two longer (105% and 110%) than the designed wavelength. As Figure 5 shows, the loss of contrast occurs at wavelengths shorter than about 90% and longer than 105% of the design point.

6. Conclusions

In this paper we have presented a new mask concept and four specific new mask designs for high-contrast imaging. Table 1 summarizes our results in tabular form. We leave it to others to decide which of these four designs most closely matches the needs of TPF.

We end the paper by reiterating that the basic idea is similar to the apodized square aperture concept of Nisenson and Papaliolios (2001) except that we are working with pupil plane masks rather than apodizations. Also, by optimizing the design, we get high contrast everywhere outside a narrow $+$-shaped diffraction spike whereas the Nisenson and Papaliolios designs provide high contrast only in a neighborhood of the two diagonals.

Acknowledgements. We are grateful for the continuing support we have received for this work from NASA and JPL. The first author also wishes to acknowledge support from the NSF (CCR-0098040) and the ONR (N00014-98-1-0036).

REFERENCES

N. J. Kasdin, R. J. Vanderbei, M. G. Littman, and D. N. Spergel. Optimal asymmetric apodizations and shaped pupils for planet finding coronagraphy. *submitted*, 2004.

N.J. Kasdin, R.J. Vanderbei, D.N. Spergel, and M.G. Littman. Extrasolar Planet Finding via Optimal Apodized and Shaped Pupil Coronagraphs. *Astrophysical Journal*, 582:1147–1161, 2003.

M. J. Kuchner and W. A. Traub. A coronagraph with a band-limited mask for finding terrestrial planets. *The Astrophysical Journal*, (570):900+, 2002.

P. Nisenson and C. Papaliolios. Detection of earth-like planets using apodized telescopes. *The Astrophysical Journal*, 548(2):L201–L205, 2001.

D. N. Spergel. A new pupil for detecting extrasolar planets. *astro-ph/0101142*, 2000.

R.J. Vanderbei, N.J. Kasdin, and D.N. Spergel. New pupil masks for high-contrast imaging. In *Proceedings of SPIE Conference on Astronomical Telescopes and Instrumentation*, number 07 in 5170, 2003a.

R.J. Vanderbei, D.N. Spergel, and N.J. Kasdin. Spiderweb Masks for High Contrast Imaging. *Astrophysical Journal*, 590:593–603, 2003b.

R.J. Vanderbei, D.N. Spergel, and N.J. Kasdin. Circularly Symmetric Apodization via Starshaped Masks. *Astrophysical Journal*, 599:686–694, 2003c.

This preprint was prepared with the AAS LaTeX macros v5.2.

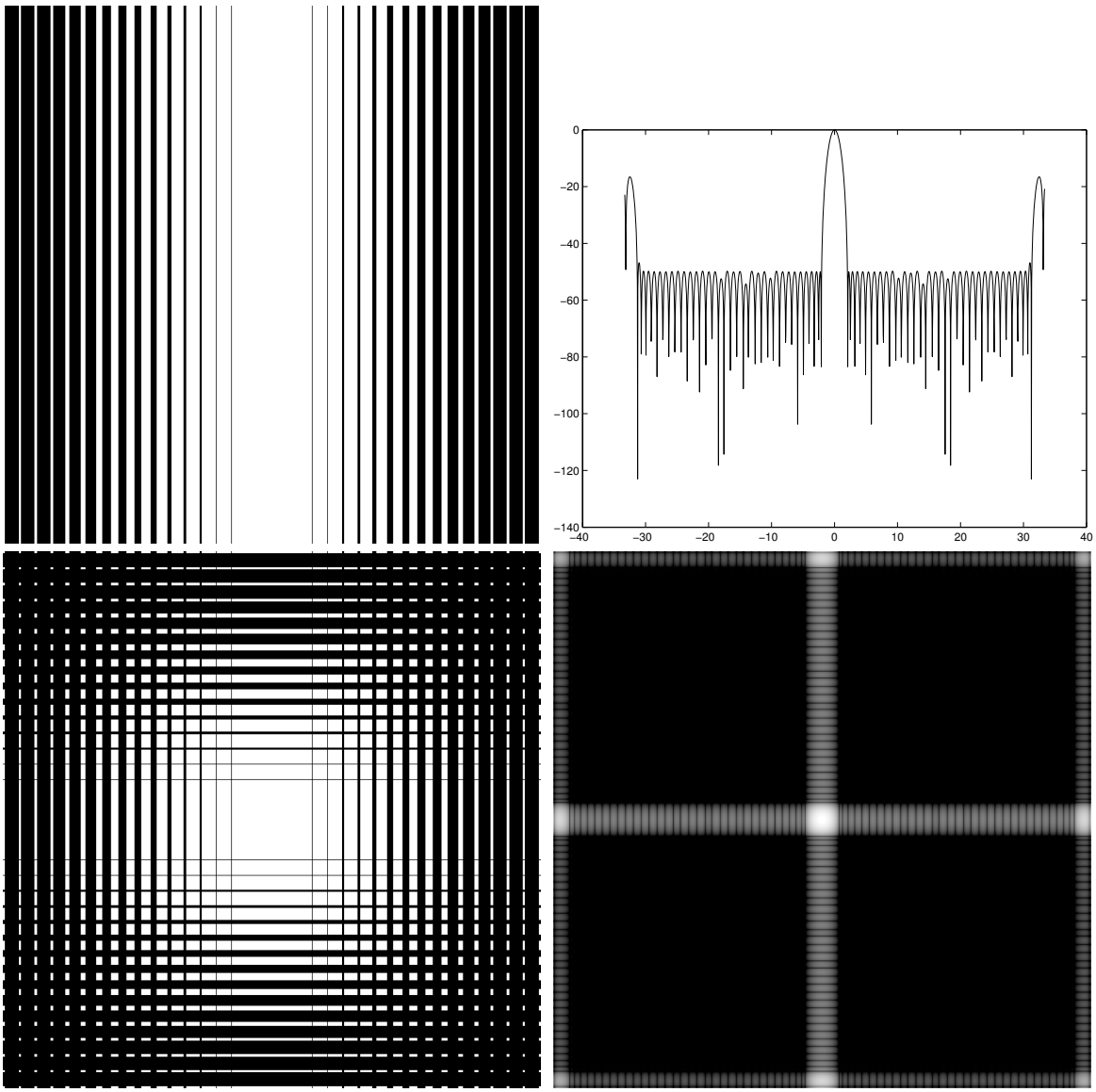

Fig. 1.— *A simple checkerboard mask.* The open area of the checkerboard mask is 28.1% and the Airy throughput is 15.1%. *Top left.* A barcode mask designed to provide 10^{-5} contrast from $2\lambda/D$ to $25\lambda/D$. *Top right.* The PSF associated with the barcode mask. *Bottom left.* The corresponding checkerboard mask. *Bottom right.* The PSF corresponding to the checkerboard mask. The gray-scale represents a logarithmic stretch with black corresponding to 10^{-10} and white corresponding to 1.

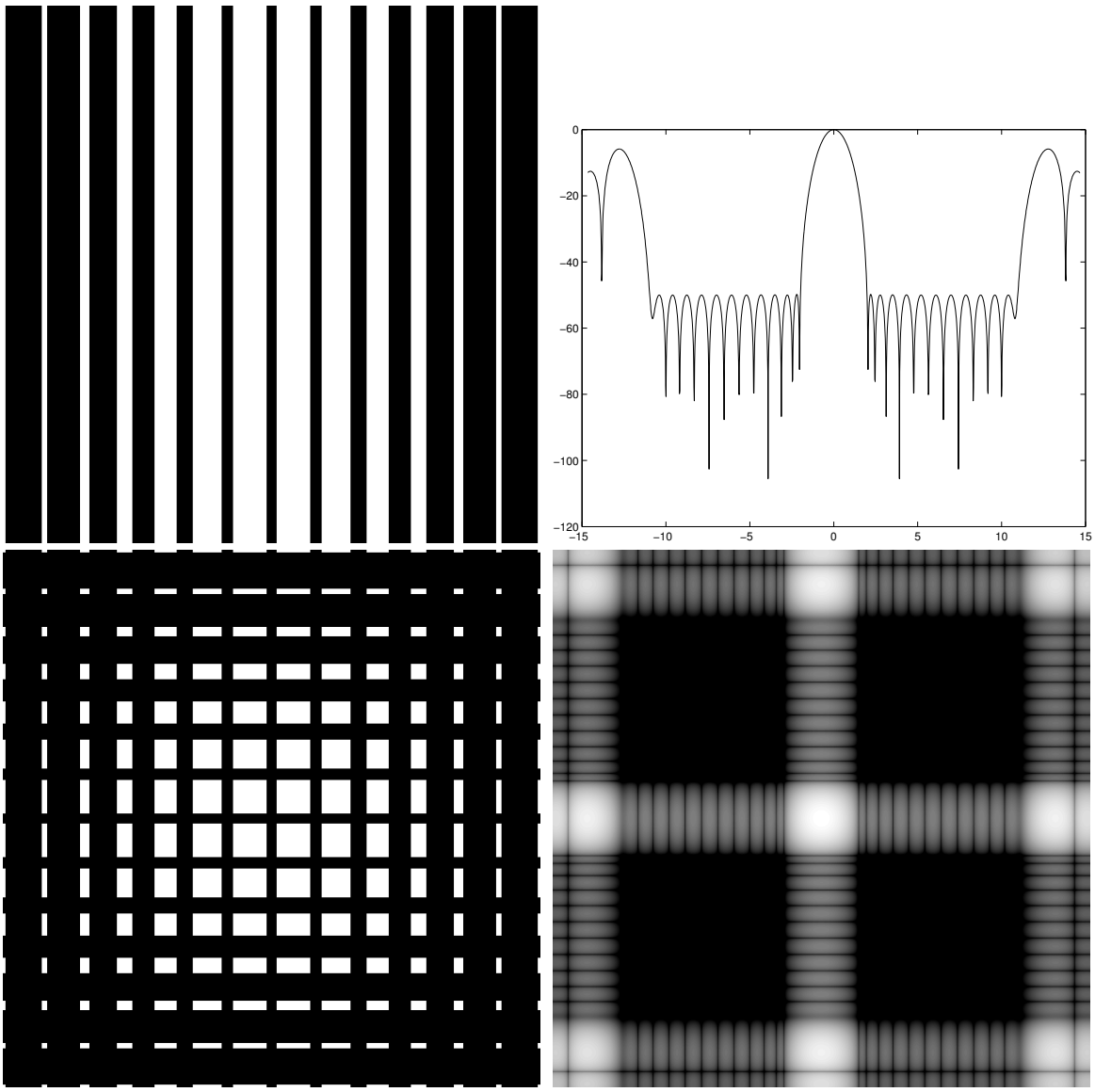

Fig. 2.— *A centrally-obstructed checkerboard mask.* This design includes a 2% central stripe to hang/hide a secondary mirror. The open area of the checkerboard mask is 17.2% and the Airy throughput is 5.3%. *Top left.* A barcode mask designed to provide 10^{-5} contrast from $2\lambda/D$ to $11\lambda/D$. *Top right.* The PSF associated with the barcode mask. *Bottom left.* The corresponding checkerboard mask. *Bottom right.* The PSF corresponding to the checkerboard mask. The gray-scale represents a logarithmic stretch with black corresponding to 10^{-10} and white corresponding to 1.

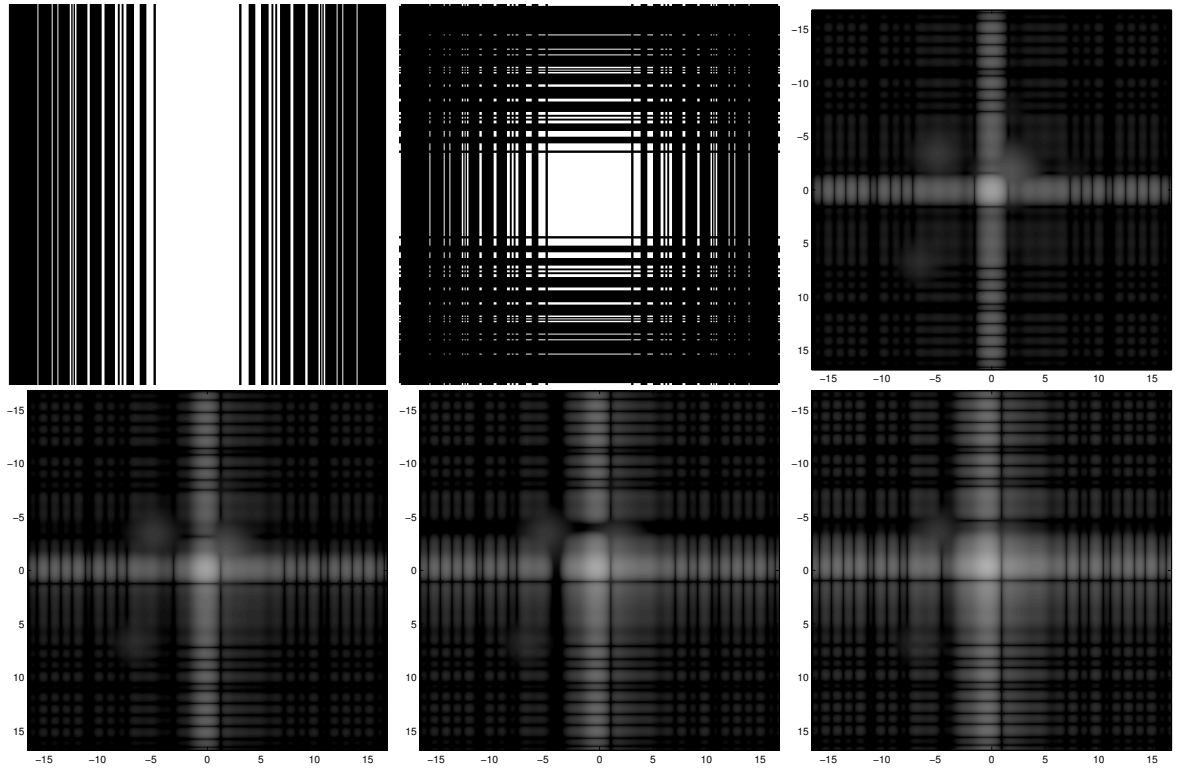

Fig. 3.— *A Lyot-style coronagraph.* A simulated 3-planet star system as it would appear in a Lyot-style coronagraph in which the entrance pupil is an open square, the first image plane has a "plus" shaped occulter of half-width $0.6\lambda/D$, and a checkerboard mask in the Lyot plane. *Top left.* A barcode mask designed to provide 10^{-5} contrast from $1.4\lambda/D$ to $21\lambda/D$ when used in conjunction with the image-plane occulter. *Top middle.* The corresponding checkerboard mask. The Airy throughput for this mask is 6.2%. *Top right.* The simulated image. The planet in the upper right quadrant is located at $(1.7, 1.7)$ and is 10^{-8} times as bright as the star. The planet in the upper left quadrant is located at $(-5.1, 3.4)$ and is 10^{-9} times as bright as the star. The planet in the lower left quadrant is located at $(-6.8, -6.8)$ and is 3×10^{-10} times as bright as the star. The gray-scale image is logarithmically stretched to highlight the faint planets. *Bottom.* The effect of pointing error. From left to right, the pointing error is 0.048, 0.096, and 0.144. The direction of the error is along the diagonal into the first quadrant.

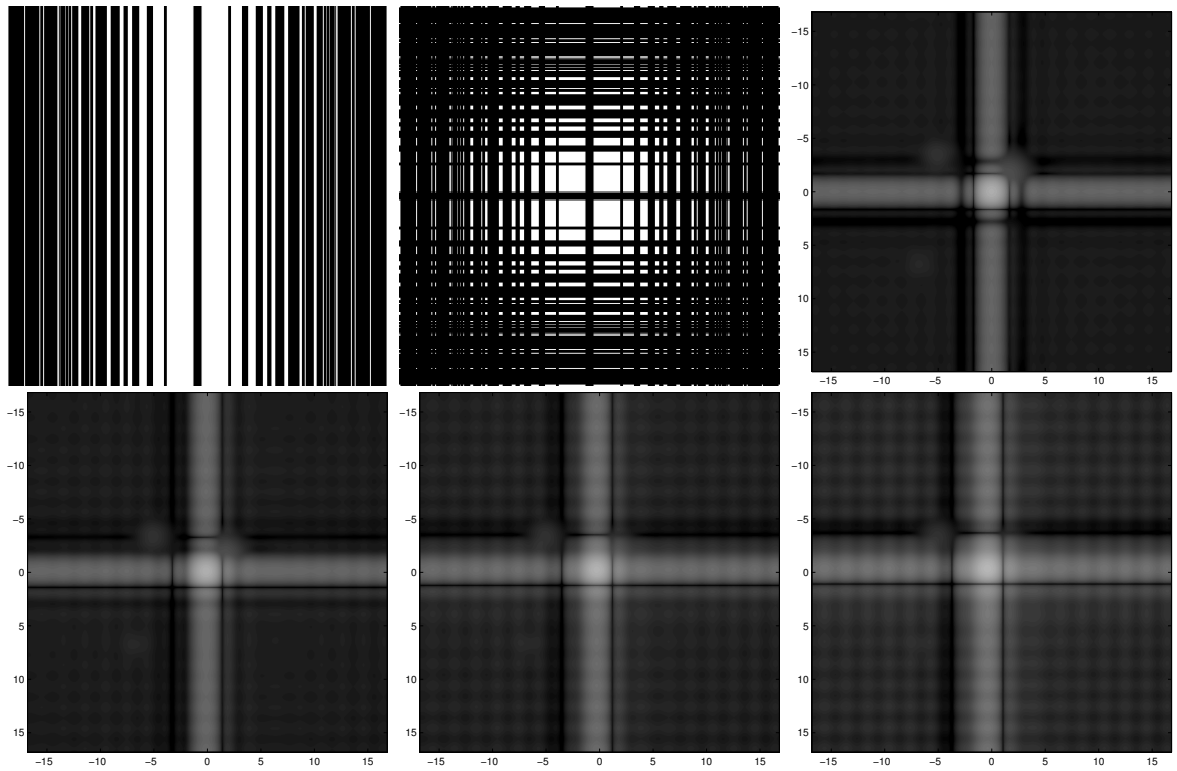

Fig. 4.— *A centrally-obstructed Lyot-style coronagraph.* A simulated 3-planet star system as it would appear in a Lyot-style coronagraph in which the entrance pupil is an open square with a plus-sign spider, the first image plane has a "plus" shaped occulter of half-width $0.6\lambda/D$, and a checkerboard mask in the Lyot plane. This design includes a 2% central obstruction. *Top left.* A barcode mask designed to provide 10^{-5} contrast from $1.4\lambda/D$ to $21\lambda/D$ when used in conjunction with the image-plane occulter. *Top middle.* The corresponding checkerboard mask. The Airy throughput for this mask is 3.5%. *Top right.* The simulated image. The planet in the upper right quadrant is located at $(1.7, 1.7)$ and is 10^{-8} times as bright as the star. The planet in the upper left quadrant is located at $(-5.1, 3.4)$ and is 10^{-9} times as bright as the star. The planet in the lower left quadrant is located at $(-6.8, -6.8)$ and is 3×10^{-10} times as bright as the star. The gray-scale image is logarithmically stretched to highlight the faint planets. *Bottom.* The effect of pointing error. From left to right, the pointing error is 0.048, 0.096, and 0.144. The direction of the error is along the diagonal into the first quadrant.

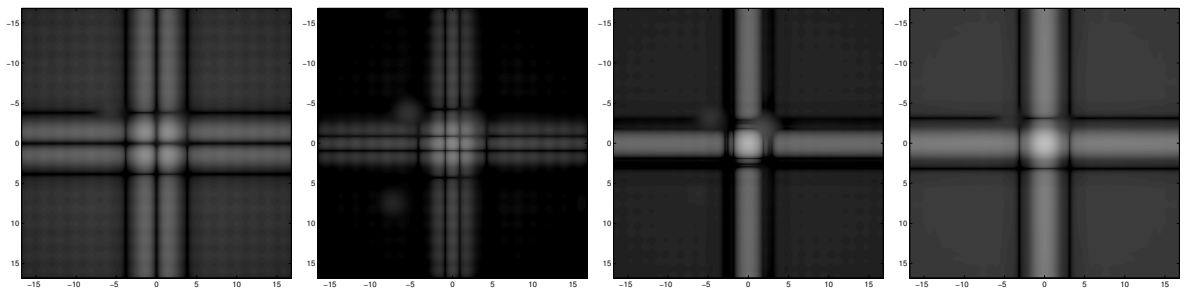

Fig. 5.— The simulated 3-planet star system as it would appear in the Lyot-style coronagraph of Figure 4 imaged at wavelengths shorter and longer than the design point. From left to right, the wavelengths are 85%, 90%, 105% and 110% of the wavelength for which the system was designed.

Description	ρ_{iwa}	ρ_{owa}	$\mathcal{T}_{Airy}$
Simple Checkerboard	$2\sqrt{2}$	25	15.1
Checkerboard with 2% Central Obstruction	$2\sqrt{2}$	11	5.3
Lyot Checkerboard	$1.4\sqrt{2}$	21	6.2
Lyot Checkerboard with 2% Central Obstruction	$1.4\sqrt{2}$	21	3.5

Table 1: Summary of the results for the specific masks considered.